

Microstructure, mechanical property and chemical property in Ni₃Al-Ni₃Ti-Ni₃Nb-based multi-intermetallic alloys

K. OHIRA, Y. KANENO, T. TAKASUGI

Department of Metallurgy and Materials Science, Graduate School of Engineering, Osaka Prefecture University, 1-1 Gakuen-cho, Sakai, Osaka 599-8531, Japan
E-mail: takasugi@mtl.osakafu-u.ac.jp

Microstructure, high-temperature compressive and tensile deformation, and corrosion property of multi-phase alloys based on Ni₃Al-Ni₃Ti-Ni₃Nb pseudo-ternary alloy system were investigated. The microstructures of these alloys were largely dependent on alloy composition but independent of annealing temperature. Alloys composed of multi-phase microstructures of L1₂, D0₂₄ and D0_a showed substantially enhanced compressive yield stress as well as a certain amount of compressive plasticity at whole temperature, while they did not show reasonable tensile elongation at whole temperature. Also, alloys composed of lamellar-like multi-phase microstructures are effective in enhancing compressive yield stress particularly at high temperature. Multi-phase alloys with low Nb contents have good corrosion resistance, especially in high concentration of sulfuric acid.

© 2004 Kluwer Academic Publishers

1. Introduction

Intermetallics have attractive properties as high temperature structural and chemical materials. Some of them have an increasing strength with increasing temperature. However, most of monolithic intermetallics have some drawbacks, such as poor ductility at room temperature and low strength at high temperature. On the other hand, it is expected that multi-phase intermetallics provide a good balance of room-temperature ductility, high-temperature strength and oxidation resistance, as understood from recent development of e.g., TiAl-based intermetallics consisting of γ and α_2 phases [1, 2]. It is known that a group of Ni₃Al, Ni₃Ti and Ni₃Nb which are called as topologically close packed (TCP) structures (phases) have been of great interest as a constituent phase in advanced intermetallics as well as a strengthener in Ni-based superalloys. They generally show high thermal, chemical and microstructural stabilities, and also attractive mechanical properties such as strength anomaly at high temperatures as well as reasonable deformability at low temperatures [3–9]. Ni₃Al has L1₂ structure with an ordered structure based on f.c.c. lattice (A1) with a lattice parameter of $a = 0.3572$ nm. Ni₃Ti has D0₂₄ structure with a tetragonal structure with a lattice parameter of $a = 0.5101$ nm and $b = 0.8307$ nm. Last, Ni₃Nb has D0_a structure with an ordered structure based on h.c.p. lattice with a parameter of $a = 0.5106$ nm, $b = 0.4251$ nm and $c = 0.4553$ nm.

Isothermal Ni₃Al-Ni₃Ti [10, 11], Ni₃Ti-Ni₃Nb [12, 13] and Ni₃Nb-Ni₃Al [14, 15] pseudo-binary phase diagrams have been reported so far. Also, an isother-

mal Ni₃Al-Ni₃Ti-Ni₃Nb pseudo-ternary phase diagram at 1273 K was recently reported by the present authors [16]. The present study shows that microstructures composed of two-phase or three-phase among Ni₃Al, Ni₃Ti and Ni₃Nb actually exist, and therefore are promising as a new class of intermetallics, i.e., the so-called Ni-based multi-phase intermetallic alloys [16]. Also, we investigate the relation between microstructure, and mechanical and chemical properties in multi-phase intermetallic alloys based on Ni₃Al-Ni₃Ti-Ni₃Nb pseudo-ternary alloy system. Particularly, multi-phase intermetallic alloys with low Ti contents and relatively high Al contents are focused, because reasonably fair balance of mechanical and chemical properties is expected in these alloys.

2. Experimental procedures

Alloys used in this study were prepared from starting raw materials of 99.9 wt%Ni, 99.99 wt%Al, 99.9 wt%Ti and 99.9 wt%Nb. Alloy button ingots mostly with a dimension of 30 mm were made by arc melting under an argon atmosphere on a copper hearth using a tungsten electrode. Alloy compositions prepared in this study are shown in Table I. The used alloy compositions are also plotted in Fig. 1, i.e., in the form of Ni₃Al-Ni₃Ti-Ni₃Nb pseudo-ternary phase diagram reported previously [16]. Also, some alloy compositions were doped with 0.01 wt% boron. All the button ingots were sectioned to a proper size along solidified direction of button ingot by an electro-discharge machine (EDM) or a precision wheel cutter. The sectioned specimens were encapsulated into silica tube and evacuated. Evacuated silica

TABLE I Chemical compositions and microstructures of alloys used in this study

Alloy	Alloy compositions					Microstructure
	Ni (at%)	Al (at%)	Ti (at%)	Nb (at%)	B (wt%)	
No. 1	75	14	1	10	–	$L1_2 - D0_a$
No. 1 + B	75	14	1	10	0.01	$L1_2 - D0_a$
No. 2	75	9	1	15	–	$L1_2 - D0_{24} - D0_a$
No. 3	75	4	1	20	–	$L1_2 - D0_{24} - D0_a$
No. 4	75	13.5	1.5	10	–	$L1_2 - D0_{24} - D0_a$
No. 4 + B	75	13.5	1.5	10	0.01	$L1_2 - D0_{24} - D0_a$
No. 5	75	11	1.5	12.5	–	$L1_2 - D0_{24} - D0_a$
No. 6	75	8.5	1.5	15	–	$L1_2 - D0_{24} - D0_a$
No. 7	75	14.5	2.5	8	–	$L1_2 - D0_{24}$
No. 7 + B	75	14.5	2.5	8	0.01	$L1_2 - D0_{24}$

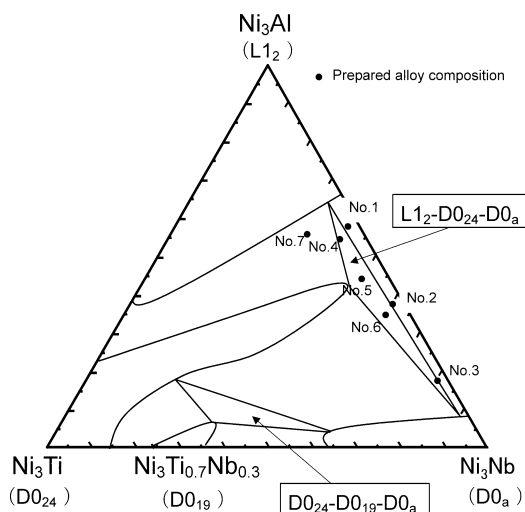


Figure 1 An isothermal $Ni_3Al-Ni_3Ti-Ni_3Nb$ pseudo-ternary phase diagram at 1273 K. Alloy compositions used in this study are plotted in this figure.

tubes were homogenized in a vacuum at 1173 K for 14 days, at 1273 K for 7 days and at 1373 K for 5 days, respectively, followed by a water quenching.

Metallographic observation was performed by optical microscopy (OM) and scanning electron microscopy (SEM) attached with wave-length dispersive spectroscopy (WDS). The determination of constituent intermetallic phases was conducted on the basis of SEM electron-probe analysis.

Compression tests at the temperature range between room temperature and 1223 K were conducted within a metal tube surrounded by an electric furnace, while those at temperatures beyond 1223 K were conducted within a vessel in which tungsten mesh heater was assembled. Tension tests at the temperature range between room temperature and 1173 K were conducted within a metal tube surrounded by an electric furnace. Compression and tension tests in both types of furnace were conducted in a vacuum degree of approximately 1.5×10^{-3} Pa. Compressive specimens with a dimension $2 \times 2 \times 5$ mm³ and tensile specimens with a gauge dimension $2 \times 1 \times 10$ mm³ were cut from the button ingots homogenized at 1373 K for 5 days. The faces of compressive and tensile specimens were abraded with a sufficiently fine SiC paper. Nominal

strain rates used in the compressive and tensile tests were 3.3×10^{-4} s⁻¹ and 1.6×10^{-4} s⁻¹, respectively. Compressive yield stress was defined at 0.2% offset strain.

Corrosion tests were performed at 363 K for 24 h in solutions of 40, 60, 80 and 98% sulfuric acid, using specimens with a dimension of $8 \times 4 \times 1$ mm³. Corrosion specimens were cut from the button ingots homogenized at 1373 K for 5 days. Before the corrosion measurement, all surfaces were abraded with 1500-grid SiC paper. The corrosion property was evaluated by mass loss per hour.

3. Results and discussion

3.1. Microstructure

Fig. 2 shows back scattering (BS)-SEM microstructures of alloys homogenized at 1373 K for 5 days. Alloy Nos. 2, 3, 4, 5 and 6 are composed of a three-phase microstructure of $L1_2 + D0_{24} + D0_a$. Alloy Nos. 1 and 7 are composed of two-phase microstructures of $L1_2 + D0_a$ and $L1_2 + D0_{24}$, respectively. Phases determined for each alloy are also shown in Table I. All the alloys more or less consist of dendrite structure, resulting from the influence of heat flow from bottom to top of the button ingot (i.e., solidification direction). For alloy Nos. 2 and 6 with high Nb contents, two-phase region with a lamellar-like microstructure composed of $D0_{24} + D0_a$ is mixed with three-phase region in which finely dispersed equiaxed-like grains composed of $L1_2 + D0_{24} + D0_a$ are observed. For alloy No. 4 with high Al content, three-phase region with finely dispersed equiaxed-like grains composed of $L1_2 + D0_{24} + D0_a$ exists between primary $L1_2$ dendrites. For alloy No. 5, three-phase region with finely dispersed equiaxed-like grains composed of $L1_2 + D0_{24} + D0_a$ exists between primary $D0_{24}$ dendrites. Alloy Nos. 1 and 7 exhibit dendrite structure composed of $L1_2 + D0_a$ and $L1_2 + D0_{24}$, respectively.

The microstructures of these alloys homogenized at 1173 K for 14 days, 1273 K for 7 days and 1373 K for 5 days were similar one another from morphological point of view. Thus, the observed morphology does not depend on heat treatment condition but depends on alloy composition. This result indicates that any invariant reaction does not occur in the observed alloy concentrations and at the temperature region between 1373 and 1173 K, and significant solubility changes do not exist in each constituent phase. Also, it is noted that the boron-doping by an amount of 0.01 wt% does not affect the microstructures.

3.2. Mechanical property

Fig. 3 plots compressive yield stress as a function of test temperature for alloys composed of a three-phase microstructure of $L1_2 + D0_{24} + D0_a$. Here, the data for Ni_3Al binary alloy [17] are plotted for reference. It has been observed that as temperature increases the yield stress of Ni_3Al [3–6], Ni_3Ti [7, 9] and Ni_3Nb [8] binary alloys increases, and then shows a peak, followed by a rapid decrease. Actually, alloy No. 2 showed a peak of yield stress at intermediate temperature. The yield

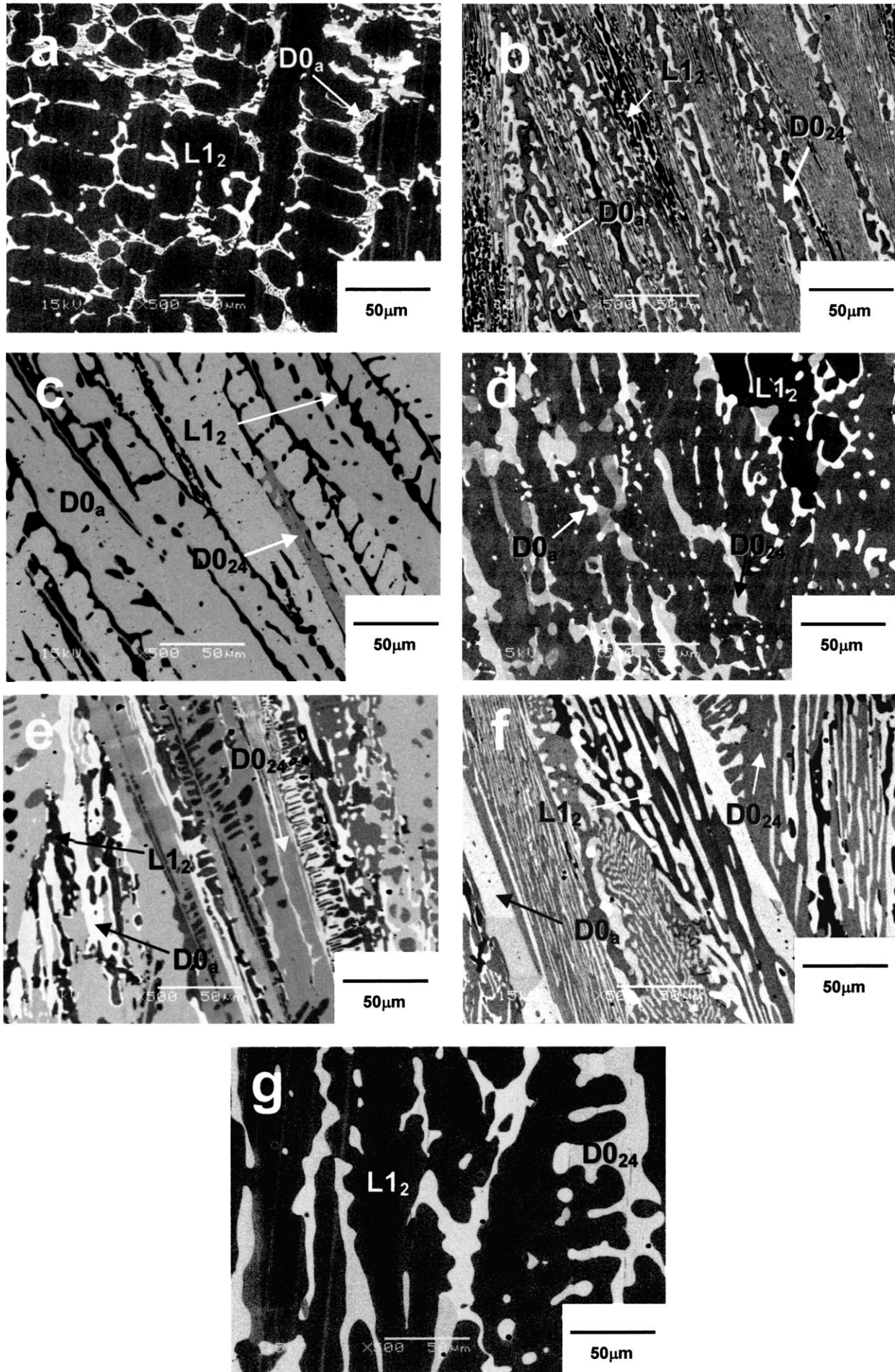


Figure 2 BS-SEM microstructures of alloys (a) No. 1, (b) No. 2, (c) No. 3, (d) No. 4, (e) No. 5, (f) No. 6 and (g) No. 7, which were homogenized at 1373 K for 5 days. Note that the constituent L1₂, D0₂₄ and D0_a phases are imaged as black, gray and white colors, respectively.

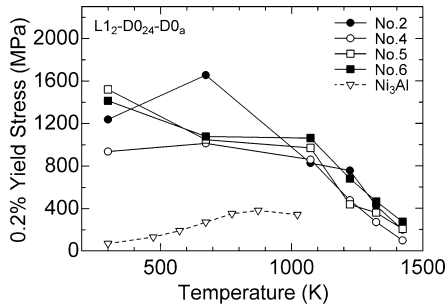


Figure 3 Compressive yield stress as a function of test temperature for alloys (Nos. 2, 4, 5 and 6) composed of a three-phase microstructure of $L1_2 + D0_{24} + D0_a$. Data of Ni_3Al binary alloy were also included for reference [17].

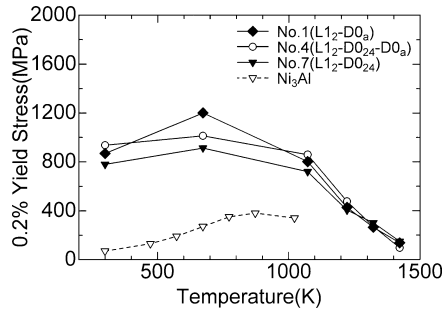


Figure 4 Compressive yield stress as a function of test temperature for alloys (Nos. 1, 4 and 7) with high Al contents. Note that these alloys are composed of different microstructures of $L1_2 + D0_a$, $L1_2 + D0_{24} + D0_a$ and $L1_2 + D0_{24}$, respectively. Date of Ni_3Al binary alloy was also included for reference [17].

stress level of the measured multi-phase alloys was substantially high particularly at low temperatures, in comparison with that of Ni_3Al binary alloy, and remained high up to about 1100 K, followed by rapid decrease at temperature beyond about 1100 K. It appears that the yield stress at low temperatures is closely related to the volume fraction of the constituent phases and their morphology. Also, it is noted that the yield stress

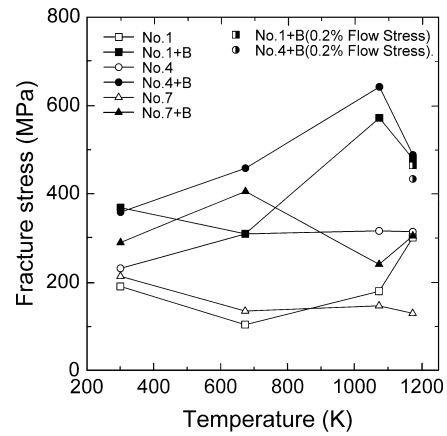


Figure 6 Tensile fracture stress as a function of test temperature for boron-doped and -undoped alloys (Nos. 1, 4 and 7) with high Al contents. Note that these alloys are composed of different microstructures of $L1_2 + D0_a$, $L1_2 + D0_{24} + D0_a$ and $L1_2 + D0_{24}$, respectively.

of alloy Nos. 2 and 6 with a lamellar-like microstructure is higher at temperature beyond 1223 K than that of other alloys.

Fig. 4 shows compressive yield stress as a function of test temperature for alloys with similarly high Al contents (i.e., alloy Nos. 1, 4 and 7). Alloy Nos. 1 and 7 are composed of two-phase microstructures, i.e., $L1_2 + D0_a$ and $L1_2 + D0_{24}$, respectively, while alloy No. 4 is composed of a three-phase microstructure of $L1_2 + D0_{24} + D0_a$, as already shown in Fig. 3. However, the grain morphology of these alloys is similar and consists of large dendrite structure. The yield stress of these alloys is nearly identical at the whole test temperatures, but certainly higher than that of Ni_3Al . Also, it is noted that the yield stress levels of these alloys are generally lower at low temperatures below 1100 K than those of the previous group of alloys composed of a three-phase microstructure (i.e., Fig. 3). It is pointed out from Figs 3 and 4 that alloys composed of a lamellar-like microstructure are stronger particularly

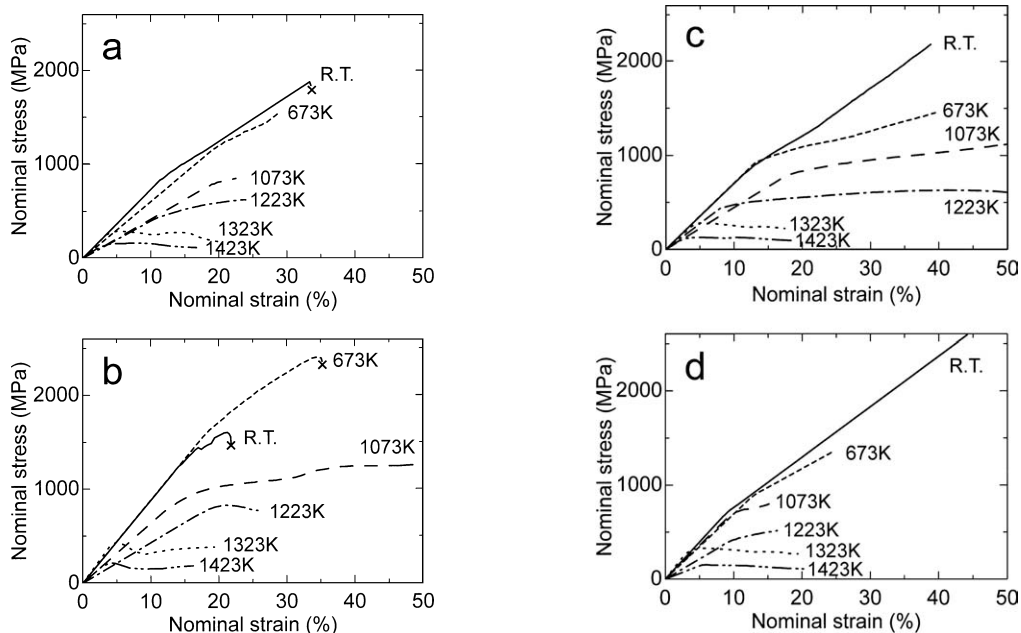


Figure 5 Changes of nominal stress vs. nominal strain curve with temperature for alloys (a) No.1, (b) No. 2, (c) No. 4 and (d) No. 7. The deformation was performed by compression. Note that cross marks mean rupturing.

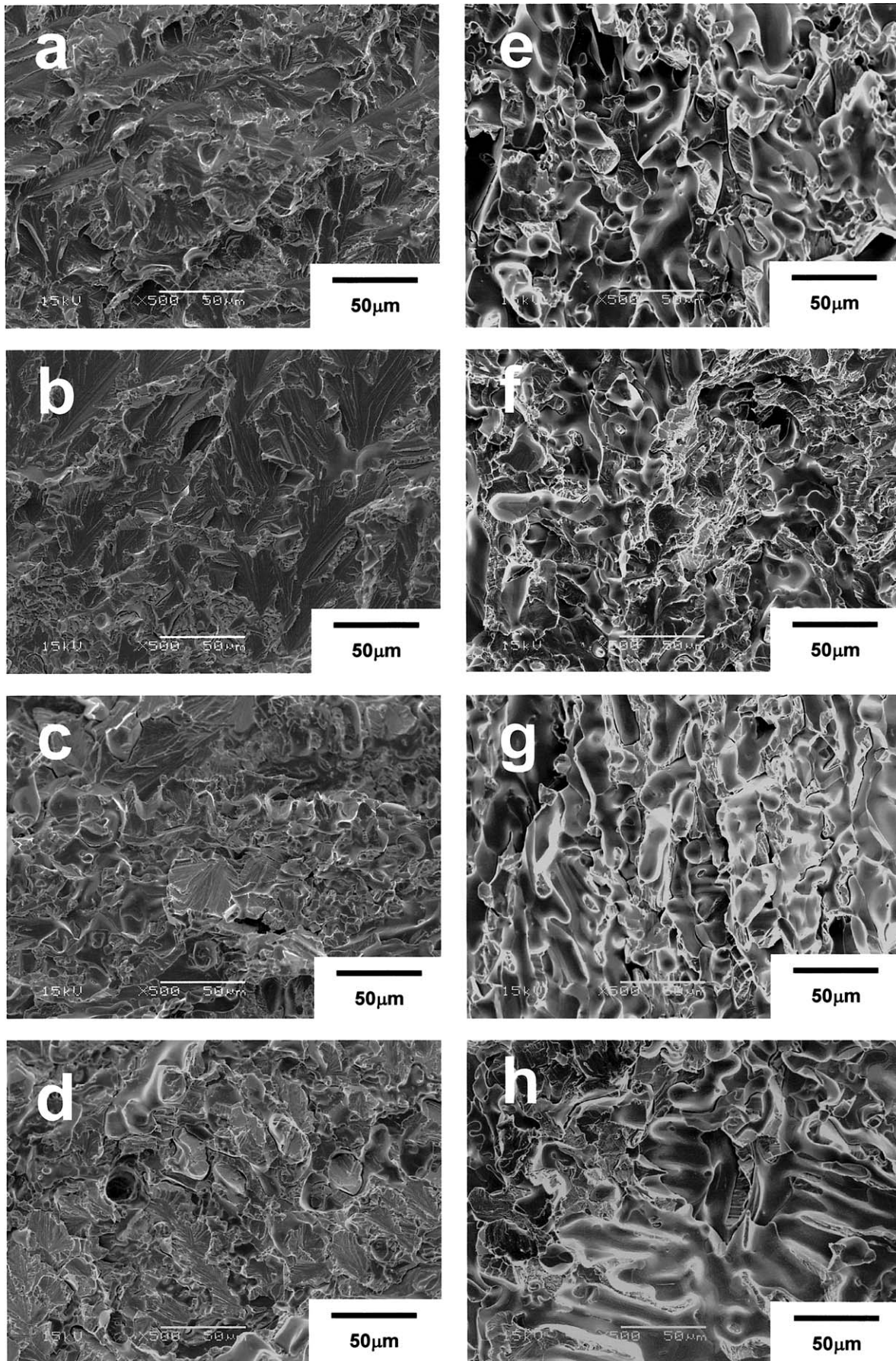


Figure 7 SEM fractography as a function of test temperature for boron-doped (No. 4+B) (a, b, c, d) and -undoped (No. 4) (e, f, g, h) alloys with high Al content, respectively. The observation was conducted on the specimen tensile-deformed at room temperature (a, e), 673 K (b, f), 1073 K (c, g) and 1173 K (d, h), respectively.

at high temperatures than those composed of dendrite structure.

Fig. 5 shows changes of nominal stress versus nominal strain curves with temperature for alloy Nos. 1, 2, 4 and 7. Depending on alloy composition and temperature, largely different stress versus strain curves were observed. At room temperature, alloy composed of a lamellar-like microstructure (i.e., alloy No. 2) drew a very limited plastic flow after yielding, and then quickly ruptured. The remaining alloys (Nos. 1, 4 and 7) with high Al contents drew certain amount of plastic deformation with a large strain-hardening rate after yielding. Thus, alloys with high Al contents are ductile at low temperature, comparing with alloys with low Al contents. This result may be associated with the large volume fraction of Ni₃Al phase, which is more ductile than Ni₃Nb (D0_a) or Ni₃Ti (D0₂₄). At intermediate temperatures (room temperature—1223 K), these alloys drew moderate plastic deformation with a moderate strain-hardening rate, and then ruptured. At high temperatures (beyond 1223 K), all the alloys drew steady-state flow after yielding, indicating high plastic deformability.

Fig. 6 shows fracture stress as a function of test temperature for boron-doped and -undoped alloys with similarly high Al contents (i.e., alloy Nos. 1, 4 and 7). In tensile deformation, yielding and subsequent plastic elongation were generally not observed for even boron-doped alloys at a wide range of test temperature. However, it was found that the boron-doping is effective in enhancing fracture stress of all the alloys tested, and resulted in yielding and resultant plastic elongation at the highest temperature tested (1173 K) for alloy Nos. 1 and 4. Fig. 7 shows SEM fractography as a function of test temperature for boron-doped (No. 4 + B) and -undoped (No. 4) alloys with high Al content. It is clearly shown that the boron-doping significantly affects the fractography while test temperature does not so much affect the fractography. The boron-doping altered the fracture mode from interfacial or grain boundary fracture to cleavage-like fracture, meaning that boron enriches on interfacial planes or grain boundaries of the constituent phases.

3.3. Corrosion property

Table II shows corrosion property of some alloys in various concentration of sulfuric acid. All the alloys have a good corrosion resistance to high concentration of sulfuric acid, indicating that passive state is formed at high concentration of sulfuric acid. However, corrosion resistance to low concentration of sulfuric acid may be not so good. Alloy Nos. 1, 4 and 7 with high Al

TABLE II Mass loss of some alloys at 363 K for 24 h in various concentration of sulfuric acid (g/m² h)

Alloy	Content of sulfuric acid			
	40%	60%	80%	98%
No. 1	7.16	1.42	0	0.46
No. 4	17.59	1.86	0.91	0.90
No. 6	24.59	10.97	0.93	1.41
No. 7	12.53	1.82	0	0

contents have a better corrosion resistance than alloy No. 6 with high Nb content. This result means that a replacement of Al with Nb results in inferior corrosion property in the present alloy system and microstructure. Also, it is noted that the corrosion property measured in the present study (i.e., multi-phase intermetallic alloys based on Ni₃Al-Ni₃Ti-Ni₃Nb) is comparable to that of Ni₃Si alloys containing Cr [18].

4. Conclusions

Microstructure, high-temperature compressive and tensile stress, and corrosion property of multi-phase alloys based on Ni₃Al-Ni₃Ti-Ni₃Nb pseudo-ternary alloy system were investigated by OM, XRD, SEM, mechanical test and corrosion measurement. The obtained results are summarized as follows.

- (1) The microstructures of these alloys were largely dependent on alloy composition but almost independent of annealing temperature.
- (2) Alloys composed of multi-phase microstructures of L1₂, D0₂₄ and D0_a showed substantially enhanced compressive yield stress as well as a certain amount of compressive plasticity at whole temperature, while they did not show reasonable tensile elongation at whole temperature.
- (3) Alloys composed of lamellar-like multi-phase microstructures are effective in enhancing compressive yield stress particularly at high temperature.
- (4) Multi-phase alloys with low Nb contents have good corrosion resistance in sulfuric acid, especially in high concentration of sulfuric acid.

Acknowledgement

This work was supported in part by the Grant-in-aid for Scientific Research (B) from the Ministry of Education, Culture, Sports and Technology.

References

1. S. C. HUANG and J. C. CHESNUTT, in "Intermetallic Compounds," Vol. 2, Practice, edited by J. H. Westbrook and R. L. Fleischer (John Wiley and Sons, West Sussex, England, 1995) p. 73.
2. Y.-W. KIM, *J. Metals* **41** (1989) 24.
3. D. P. POPE and S. S. EZZ, *Int. Mater. Rev.* **29** (1984) 136.
4. N. S. STOLOFF, *ibid.* **34** (1989) 153.
5. M. YAMAGUCHI and Y. UMAKOSHI, *Prog. Mater. Sci.* **34** (1990) 1.
6. T. SUZUKI, Y. MISHIMA and S. MIURA, *ISIJ Int.* **29** (1989) 1.
7. K. HAGIHARA, T. NAKANO and Y. UMAKOSHI, *Mater. Res. Soc. Symp. Proc.* **753** (2003) 357.
8. *Idem.*, *Acta Mater.* **48** (2000) 1469.
9. *Idem.*, *ibid.* **51** (2003) 2623.
10. P. VILLARS, A. PRINCE and H. OKAMOTO, "Handbook of Ternary Alloy Phase Diagrams" (ASTM International, 1995) p. 4195.
11. P. NASH and W. W. LIANG, *Metall. Trans. A* **16** (1983) 319.
12. P. VILLARS, A. PRINCE and H. OKAMOTO, "Handbook of Ternary Alloy Phase Diagrams" (ASTM International, 1995) p. 12805.
13. M. YAMANAKA, C. YAMAUCHI, M. TAKEYAMA and T. MATSUO, *CAMPISIJ* **12** (1999) 47.

14. P. VILLARS, A. PRINCE and H. OKAMOTO, "Handbook of Ternary Alloy Phase Diagrams" (ASTM International, 1995) p. 4118.
15. M. GHANEM, N. MIURA, T. UYAMA, M. TAKEYAMA and T. MASTSUO, Collected Abstract of 1997 Fall Meeting of Japan Inst. Metals, p. 388.
16. K. TOMIHISA, Y. KANENO and T. TAKASUGI, *Intermetallics* **10** (2002) 247.
17. O. NOGUCHI, Y. OYA and T. SUZUKI, *Metall. Trans. A* **12** (1981) 1647.
18. T. TAKASUGI, H. KAWAI and Y. KANENO, *Mater. Sci. Eng. A* **329-331** (2002) 446.

*Received 4 September 2003
and accepted 12 January 2004*